AIAA 2003-2129

Wind Tunnel Testing of Various Disk-Gap-Band Parachutes

J. R. Cruz, R. E. Mineck, D. F. Keller,
and M. V. Bobskill
NASA Langley Research Center
Hampton, VA

17th AIAA Aerodynamic Decelerator Systems Technology Conference and Seminar
19–22 May 2003
Monterey, California

WIND TUNNEL TESTING OF VARIOUS DISK-GAP-BAND PARACHUTES

Juan R. Cruz,* Raymond E. Mineck,† Donald F. Keller,‡ and Maria V. Bobskill§
NASA Langley Research Center
Hampton, Virginia

ABSTRACT

Two Disk-Gap-Band model parachute designs were tested in the NASA Langley Transonic Dynamics Tunnel. The purposes of these tests were to determine the drag and static stability coefficients of these two model parachutes at various subsonic Mach numbers in support of the Mars Exploration Rover mission. The two model parachute designs were designated 1.6 Viking and MPF. These model parachute designs were chosen to investigate the tradeoff between drag and static stability. Each of the parachute designs was tested with models fabricated from MIL-C-7020 Type III or F-111 fabric. The reason for testing model parachutes fabricated with different fabrics was to evaluate the effect of fabric permeability on the drag and static stability coefficients. Several improvements over the Viking-era wind tunnel tests were implemented in the testing procedures and data analyses. Among these improvements were corrections for test fixture drag interference and blockage effects, and use of an improved test fixture for measuring static stability coefficients. The 1.6 Viking model parachutes had drag coefficients from 0.440 to 0.539, while the MPF model parachutes had drag coefficients from 0.363 to 0.428. The 1.6 Viking model parachutes had drag coefficients 18 to 22 percent higher than the MPF model parachute for equivalent fabric materials and test conditions. Model parachutes of the same design tested at the same conditions had drag coefficients approximately 11 to 15 percent higher when manufactured from F-111 fabric as compared to those fabricated from MIL-C-7020 Type III fabric. The lower fabric permeability of the F-111 fabric was the source of this difference. The MPF model parachutes had smaller absolute statically stable trim angles of attack as compared to the 1.6 Viking model parachutes for equivalent fabric materials and test conditions. This was attributed to the MPF model parachutes' larger band height to nominal diameter ratio. For both designs, model parachutes fabricated from F-111 fabric had significantly greater statically stable absolute trim angles of attack at equivalent test conditions as compared to those fabricated from MIL-C-7020 Type III fabric. This reduction in static stability exhibited by model parachutes fabricated from F-111 fabric was attributed to the lower permeability of the F-111 fabric. The drag and static stability coefficient results were interpolated to obtain their values at Mars flight conditions using total porosity as the interpolating parameter.

SYMBOLS AND ACRONYMS

A_{block}	vent blockage induced by test fixture requirements
A_G	gap area
A_V	vent area
c_e	effective fabric porosity
C_D	drag coefficient
$(C_D A)_{strut}$	strut drag area upstream of the model parachute at zero angle of attack
C_m	moment coefficient
C_N	normal force coefficient
C_p	pressure coefficient
C_T	tangential force coefficient
D	drag force
D_B	band diameter
D_D	disk diameter
D_{meas}	measured drag force uncorrected for strut interference effects
D_P	projected diameter
D_V	vent diameter
D_0	parachute nominal diameter
H_B	band height
H_G	gap height
k_q	dynamic pressure blockage correction factor
k_S	strut drag interference factor at zero angle of attack
k_α	strut angle of attack drag interference factor
$k_{\alpha S}$	strut drag interference factor as a function of angle of attack
k_1, k_2	constants used in the determination of c_e
L	distance from the parachute suspension lines confluence point to the apex
L_{rear}	distance from the rear balance moment center to the apex of the model parachute
L_S	suspension line length

* Aerospace Engineer; Juan.R.Cruz@nasa.gov
† Aerospace Engineer; Raymond.E.Mineck@nasa.gov
‡ Aerospace Engineer; Donald.F.Keller@nasa.gov
§ Aerospace Engineer; Maria.V.Bobskill@nasa.gov

m	moment about the suspension lines confluence point
M	Mach number
M_{rear}	moment measured by the rear wind tunnel balance about its moment center
N	normal force
N_{front}	normal force component measured by the front wind tunnel balance
N_{rear}	normal force component measured by the rear wind tunnel balance
q	dynamic pressure
q_{meas}	dynamic pressure uncorrected for blockage effects
Re^*	Reynolds number per unit length based on V_{fict}
S_P	parachute projected area
S_0	parachute nominal area
T	tangential force
T_{front}	tangential force component measured by the front wind tunnel balance
T_{rear}	tangential force component measured by the rear wind tunnel balance
V_{fict}	fictitious velocity used in the calculation of the effective fabric porosity
V_∞	free-stream velocity
X_{cp}	parachute center of pressure
α	angle of attack
α_{trim}	statically stable trim angle of attack
λ_g	geometric porosity
λ_t	total porosity
μ	fluid viscosity
ρ	fluid density

CFM	Cubic Feet per Minute
DGB	Disk-Gap-Band
EDL	Entry/Descent/Landing
LaRC	Langley Research Center
MER	Mars Exploration Rover
MPF	Mars Pathfinder
ETT	Electric Turntable
TDT	Transonic Dynamics Tunnel

INTRODUCTION

A wind tunnel test of two candidate parachute designs for the Mars Exploration Rover (MER) mission was conducted in the Transonic Dynamics Tunnel (TDT) at the NASA Langley Research Center (LaRC). Data to calculate both drag and static stability coefficients (i.e., C_D, C_T, C_N, and C_m) were collected. The model parachutes tested were of the Disk-Gap-Band (DGB) type used by the Viking[1] and Mars Pathfinder[2] missions. These model parachutes were named 1.6 Viking and MPF (Mars Pathfinder) for reasons discussed later. Since fabric permeability has an important effect on both drag and static stability, each parachute design was tested with models manufactured from fabrics with very different permeabilities: either MIL-C-7020 Type III or F-111 fabric. The parachute models fabricated from MIL-C-7020 Type III fabric exhibited higher effective fabric permeability (and total porosity for a given design) than that expected for the full-scale MER parachute at Mars flight conditions. Conversely, the parachute models fabricated from F-111 fabric had lower effective fabric permeability than that expected for the full-scale MER parachute at Mars flight conditions. With these data, values for the various coefficients were interpolated using the experimental results and taking into consideration the effective fabric permeability of the full-scale MER parachute at Mars flight conditions.

The Mars flight conditions of interest were those at heatshield release and terminal descent during the MER entry/descent/landing (EDL) sequence.[3] These conditions occur at nominal Mach numbers of approximately 0.47 and 0.29, respectively. Most of the wind tunnel test results reported herein were conducted at these Mach numbers. To capture the effects of the backshell wake on the model parachute aerodynamics, a model of the backshell was placed upstream of the model parachutes during testing.

The tests described here were similar to those conducted previously in the TDT in support of the Viking mission.[4] However, several key improvements in the test techniques and data analyses were made during the present investigation. Corrections were incorporated to account for blockage and strut drag interference effects. The effect of fabric permeability was taken into account in calculating the values of the various aerodynamic coefficients for Mars flight operations. Finally, static stability coefficients (which were not measured during the previous Viking-era wind tunnel tests in the TDT) were obtained using a new test fixture that minimized undesired interference effects.

FULL-SCALE MER PARACHUTE AND BACKSHELL

The geometry and dimensions of the full-scale MER backshell and parachute immediately after heat shield release are shown in figure 1. The dimensions shown in this figure were correct at the time the tests reported here were conducted; later in the MER program some of these dimensions were altered slightly. The parachute is attached to the backshell through a three-legged bridle and a single riser. Since the entry vehicle is spin stabilized during atmospheric entry, it may still be rotating after the parachute is deployed. The single riser is sized to absorb this rotation without twisting the parachute suspension lines. At the time the wind tunnel

tests discussed herein were conducted the full-scale MER parachute nominal diameter, D_0, was 49.5 ft and its nominal area, S_0, was 1,924 ft^2.

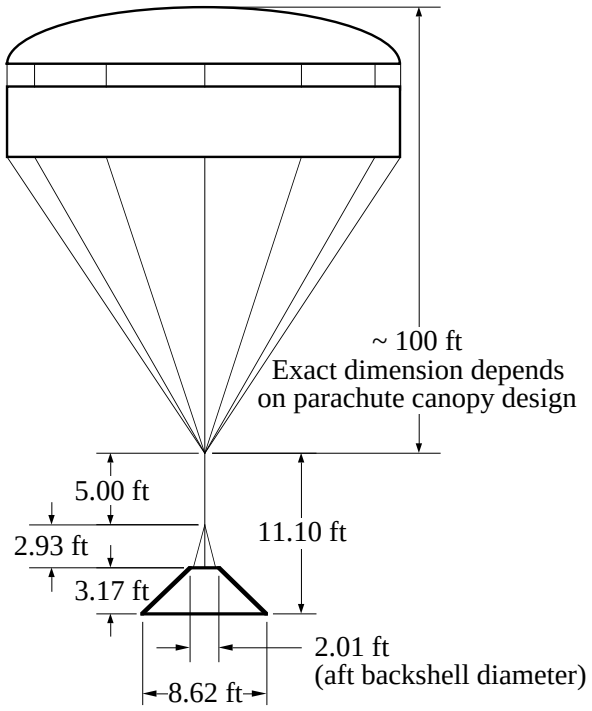

Figure 1 – Full-scale MER parachute and backshell geometry. Drawing not to scale.

TEST SETUP AND OPERATIONS

WIND TUNNEL

Testing was conducted at the NASA LaRC Transonic Dynamics Tunnel (TDT). The TDT is a closed-circuit, single-return, continuous-flow wind tunnel. It has a square 16- by 16-ft test section with cropped corners. Ten slots in the test section allow for flow expansion and transonic operation. These slots also reduce blockage effects. The TDT has a Mach number operating range from less than 0.1 to approximately 1.2. Of interest to the present research is the ability of the TDT to operate at total pressures from atmospheric (approximately 2,200 psf) to less than 50 psf. This allows for independent control of the dynamic pressure and Mach number.

To obtain the desired static stability coefficients some means of changing the angle of attack was needed. This need was met in the TDT by the Electric Turntable (ETT) mounted on the east wall of the wind tunnel (i.e., the left side when facing upstream). The ETT is usually used to change the angle of attack of aircraft semi-span models in the TDT. In the present investigation a large circular mounting plate with the test fixture was attached to the ETT inside the wind tunnel, and the ETT was commanded to hold a specified angle of attack for each test point.

PARACHUTES AND BACKSHELL MODELS

Results for two DGB model parachute designs, designated 1.6 Viking and MPF, are reported in this paper. The 1.6 Viking model parachute was a derivative of the design used by the Viking mission,[1] with a band height to nominal diameter ratio 1.6 times of that used by Viking. The MPF model parachute was a scale model of the same design as that used for the Mars Pathfinder mission.[2] These designs were chosen to explore the tradeoff between drag and static stability (mainly as determined by the statically stable trim angle of attack). All parachute models were 10.55 percent of the full-scale MER parachute at the time the testing was conducted. This yielded model parachutes with nominal diameter (D_0) and area (S_0) of 5.225 ft and 21.44 ft^2, respectively. The model parachutes' nominal diameter was chosen so as to have the same value as the Viking model parachutes previously tested in the TDT.[4] Figure 2 shows the constructed shape of a typical DGB

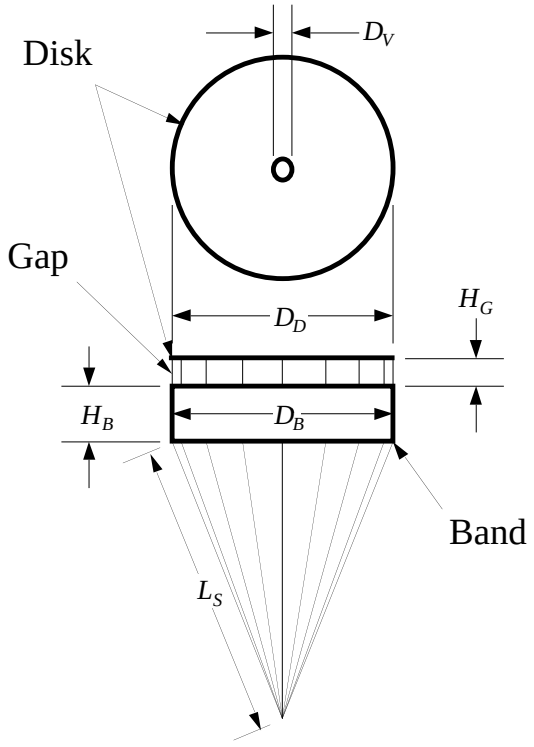

Figure 2 – Key construction parameters for a DGB parachute.

parachute. Table 1 shows the values required to define the 1.6 Viking and MPF model parachutes. Values for the Viking parachute are also included for comparison. Note the differences in band height, gap height, and vent diameter between the 1.6 Viking and MPF parachutes. The model parachutes had 40 suspension lines.

Table 1 – Geometric description of the Viking, 1.6 Viking, and MPF DGB parachutes.

	Viking	1.6 Viking	MPF
D_V/D_0	0.070	0.070	0.063
D_D/D_0	0.726	0.628	0.624
D_B/D_0	0.726	0.628	0.563
D_B/D_D	1.00	1.00	0.902
H_G/D_0	0.042	0.042	0.037
H_B/D_0	0.121	0.194	0.233
L_S	1.68 D_0	1.68 D_0	1.68 D_0
λ_g	0.127	0.112	0.092

The model parachutes were designed and fabricated by Pioneer Aerospace using either MIL-C-7020 Type III fabric (~1.6 oz/yd^2 nylon fabric with standard[¶] permeability of 100 to 160 CFM/ft^2) or F-111 fabric (nylon fabric with standard permeability of 3 to 5 CFM/ft^2). These two fabrics were used to vary the effective fabric porosity, and thus the total porosity, of a given canopy design. As described later, this variation in total porosity was used to determine the parachute performance at Mars flight conditions. Because of the small size of the model parachutes it was decided not to fabricate them as an assembly of gores. Instead, the disk and band were fabricated from four pieces of fabric, two pieces to each component. The gore seams were simulated by sewing Kevlar™ lines through the band and disk to the apex. Fabricating the model parachutes in this simplified manner caused the fabric orientation to vary between "gores" of the disk. This change in orientation is thought to have little effect on the test results. The fabric orientation on the band was constant (block direction). Figures 3, 4, and 5 show details of the model parachute construction. Due to test fixture requirements the center of the model parachute vent was blocked. In figure 4 the vent slide fitting used during static stability testing is shown installed on the model parachute vent. The load measuring rod (described later) went through the center hole of the vent slide fitting when the model parachute was installed in the static stability test fixture. During drag testing the vent slide fitting was replaced by a nylon disk which covered the same area. In order to maintain the same geometric porosity as the full-scale MER parachutes, the vent diameter were modified to account for the additional blockage caused by the vent slide fitting or nylon disk and the oversized Kevlar™ vent lines. At the suspension lines confluence point a swivel was installed to keep the suspension lines from twisting in case the model parachute rotated during testing. The suspension lines confluence point is shown in figure 5 with the two types of swivels used.

Figure 3 – Model parachute construction disk and band details.

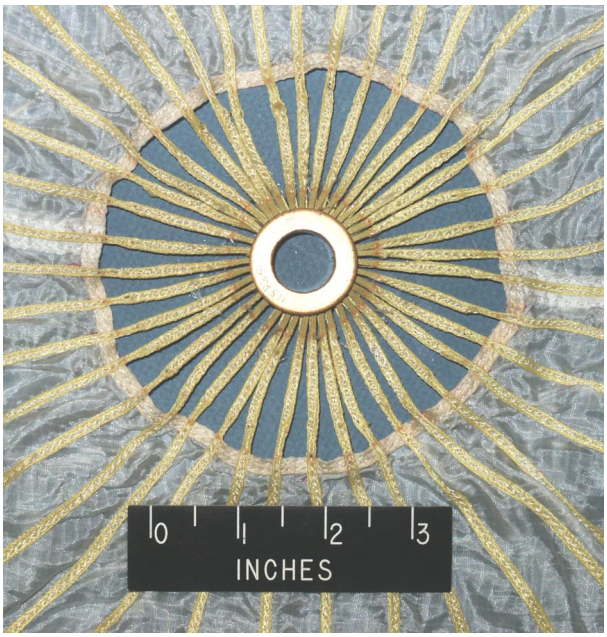

Figure 4 – Model parachute vent construction detail with the vent slide fitting used during static stability testing installed.

[¶] In this document standard permeability refers to permeability values obtained under 0.5 inch of water differential pressure in air at sea-level conditions.

It has been observed that the wake of the entry vehicle can have significant effect on parachute performance.[4] The wind tunnel testing conducted during the present research was intended to simulate events occurring after heatshield release in the MER EDL sequence. Thus, it was unnecessary to include the heatshield in the model of the entry vehicle - including just the backshell was sufficient. In addition, since the sharp upstream edge of the backshell dominated its wake, including the lander inside the backshell would have a negligible effect on the wake propagating to the model parachute canopy. Thus, the lander was not included in the backshell model. A simplified backshell model at the same 10.55 percent scale of the model parachutes was used during testing. At this scale the largest diameter of the backshell was 10.91 inches.

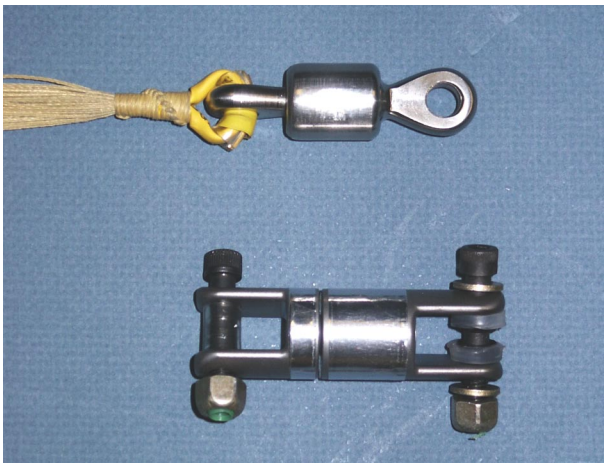

Figure 5 – Model parachute suspension lines confluence point and swivels details.

TEST FIXTURES

Two test fixtures were used during the present investigation, one to obtain data for the calculation of the drag coefficients and another to obtain data for the calculation of the static stability coefficients. These two fixtures shared common elements and were attached to the ETT through a circular mounting plate.

DRAG TEST FIXTURE

A photograph of the drag test fixture is shown in figure 6. The main elements of this test fixture were the circular mounting plate, the front truss, the wind tunnel balance, and the backshell model. The front truss was attached to the circular mounting plate. During drag testing the circular mounting plate was held at zero angle of attack. The wind tunnel balance was mounted at the end of the front truss. This wind tunnel balance was capable of measuring all force and moment components, although for drag testing only the force along the flow was of interest to determine drag. The model parachute was attached to the wind tunnel balance as shown in figures 7 and 8. Note that a swivel was mounted between the model parachute and the wind tunnel balance. This swivel allowed the model parachute to rotate without twisting the suspension lines. The wind tunnel balance was surrounded by a windshield. This windshield kept the wind tunnel balance from measuring its own drag by shielding it from the flow. The backshell model was mounted onto the windshield, yielding the desired aerodynamic wake interference with the model parachute, but not adding its own drag to that being measured by the wind tunnel balance. The drag test fixture was sized so that the attachment of the model parachute to the wind tunnel balance was at the center of the wind tunnel test section.

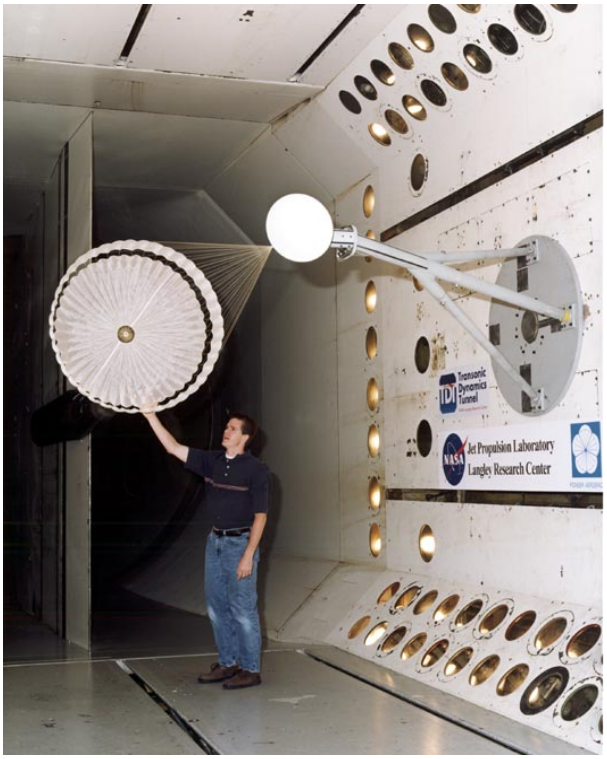

Figure 6 – Drag test fixture and model parachute.

STATIC STABILITY TEST FIXTURE

The static stability test fixture is shown in figures 9 and 10. Note that this fixture used the circular mounting plate and front truss of the drag test fixture, and added a rear truss and wind tunnel balance to

measure forces at the apex of the model parachute. During static stability testing the model parachute apex was partially constrained. Thus, by using the ETT to rotate the circular mounting plate the angle of attack of the model parachute could be set to the desired value. The front and rear trusses were designed so that the model parachute canopy was close to the axis of rotation of the ETT. By doing this the parachute canopy was maintained close to the wind tunnel centerline as the angle of attack was changed. As shown in figure 11 and 12, at the end of the rear truss there was a second wind tunnel balance capable of measuring all force and moment components. Mounted on this wind tunnel balance was a load measuring rod. Attached to the vent of the model parachute there was a fitting which slid freely on the load measuring rod (this fitting can be seen in figure 4). The forces on the apex of the model parachute were thus transmitted to, and measured by, the wind tunnel balance on the rear truss. Combining the force and moment data from the front and rear wind tunnel balances allowed for the calculation of the static stability coefficients and the model parachute length. Details on how the forces and moments were used in the calculation of these quantities is discussed in the data analysis section. In order to accommodate various model parachute lengths, the rear truss and the rear wind tunnel balance could be manually moved fore and aft.

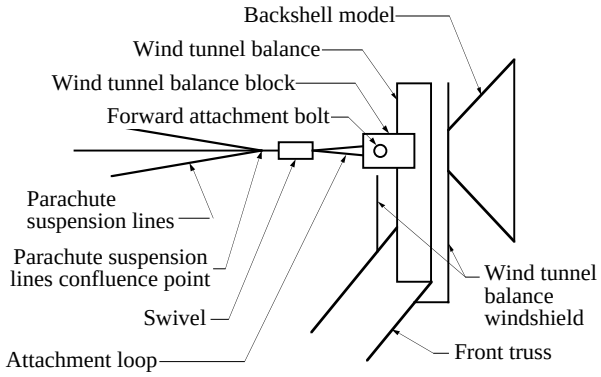

Figure 7 – Model parachute attachment to the front truss wind tunnel balance.

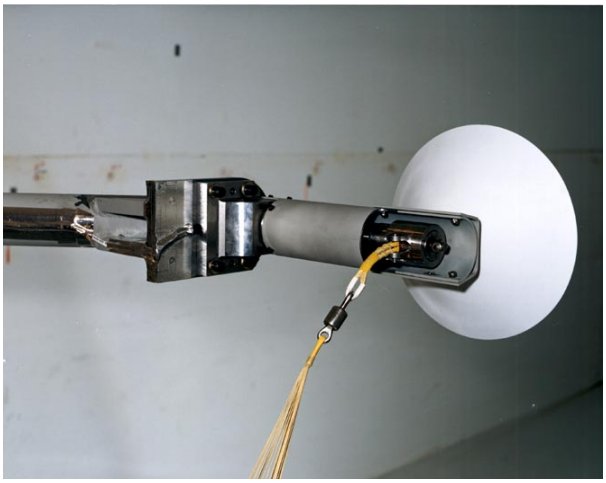

Figure 8 – Model parachute attachment to the front truss wind tunnel balance - rear view.

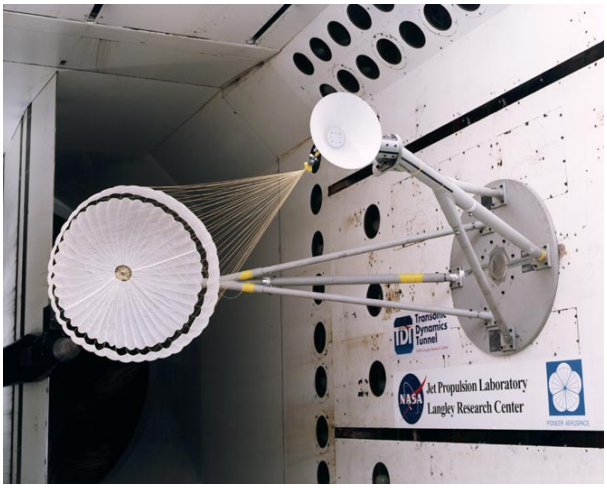

Figure 9 – Static stability test fixture with model parachute - front view.

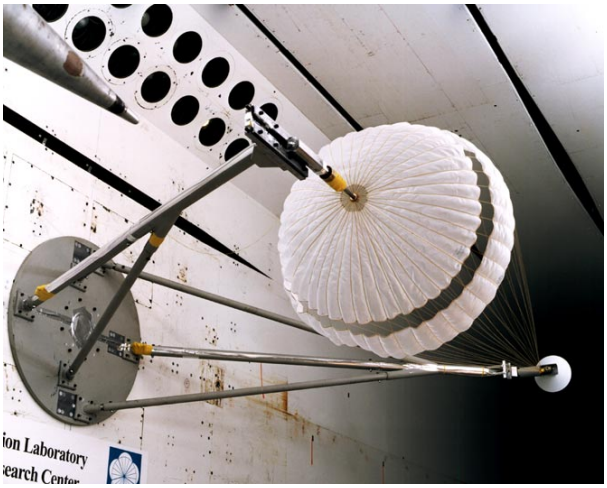

Figure 10 – Static stability test fixture with model parachute - rear view.

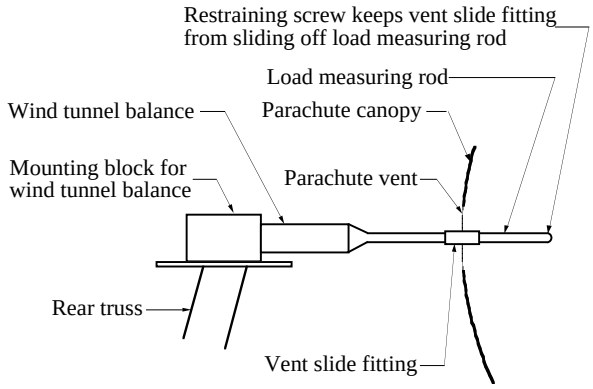

Figure 11 – Model parachute connection to the rear wind tunnel balance.

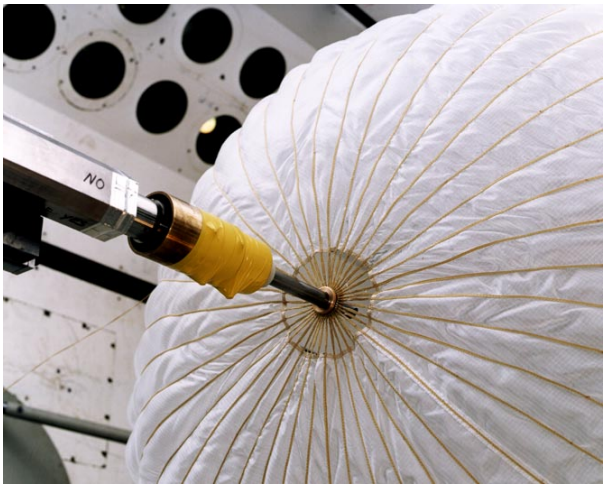

Figure 12 – Model parachute connection to the rear wind tunnel balance - rear view.

INSTRUMENTATION AND DATA ACQUISITION

The wind tunnel instrumentation consisted of total and static pressure measurements, total temperature, and wall pressures. Total pressure and total temperature were measured in the settling chamber upstream of the test section. Static pressure was measured in the plenum surrounding the test section. The wind tunnel instrumentation was used to determine dynamic pressure, Mach number, speed of sound, airspeed, density, and Reynolds number. Values of the total and static pressure were sampled by the data acquisition system at 2.5 Hz; total temperature was sampled at 3 Hz. Wall static pressures were measured at 10 locations on the east wall and at 15 locations on the west wall. The east wall pressure orifices were located 3 inches below the test section centerline between test section station 52 and test section station 70. The west wall pressure orifices were located 3 inches above the test section centerline between test section stations 52 and 80. Station locations in the TDT are measured in feet from an upstream location. The rotation axis of the ETT is at station 72. The wall pressures were measured with 1 psi, electronically scanned, differential pressure transducers referenced to the test section static pressure. The wall pressures were sampled by the data acquisition system at 10 Hz. Forces and moments from the wind tunnel balances were sampled at 100 Hz. Values of all these quantities for a given data point were reported by the data acquisition system as the average over five seconds. Multiple data points (up to 18) were collected at each test condition and/or angle of attack. The angle of attack of the static stability test fixture was determined from an electronic inclinometer mounted on the ETT. This inclinometer was sampled at 100 Hz.

Several video cameras were used to record the behavior of the model parachutes in the wind tunnel. The main use of the video from these cameras was in the determination of the inflated shape and projected diameter of the inflated model parachutes.

TEST CONDITIONS

For the present investigation the conditions of most interest to the MER mission were those at heat shield release and terminal descent during the EDL sequence. These conditions were estimated to occur at nominal Mach numbers of 0.47 and 0.29, respectively. Thus, most of the data collected was at these Mach numbers. The dynamic pressure used was typically between 25 and 27 psf. Higher values of dynamic pressure would have yielded more accurate data for two reasons. First, the dynamic pressure could be determined more accurately since it was calculated from absolute pressure transducers measuring total and static pressure. Second, higher values of the dynamic pressure induced larger forces and moments which could be measured more accurately by the wind tunnel balances. Although there were accuracy advantages to using higher dynamic pressures, model parachute durability and wind tunnel balance load limitations (usually related to dynamic loads associated with model parachute induced vibrations) limited the upper dynamic pressure for most of the tests to 27 psf. During some tests lower values of the dynamic pressure had to be used to avoid damaging the wind tunnel balances.

Before reducing wind tunnel total pressure to test at higher Mach numbers (i.e., greater than $M = 0.14$), a check-out test at sea-level pressure was typically conducted. These check-out tests were carried out at a dynamic pressure of 25 psf, yielding Mach numbers

between 0.13 and 0.14. Some of the drag results for these check-out tests are presented later in this paper.

TEST OPERATIONS

MODEL PARACHUTE INFLATION AND COLLAPSE

Prior to starting the wind tunnel during drag testing the model parachute was placed on the floor of the wind tunnel. The model parachute inflated without assistance from this position, and after repeated wind tunnel shutdowns and re-starts. For static stability testing the test fixture was rotated to an angle of attack of +10° prior to starting the wind tunnel. At this angle of attack the upstream edge of the model parachute band was facing the incoming flow. At wind tunnel startup the model parachute inflated reliably from this position and after repeated wind tunnel shutdowns and re-starts.

During one static stability test the angle of attack was increased to the point of model parachute collapse. This occurred at approximately +20° angle of attack. Reducing the angle of attack allowed the model parachute to re-inflate. However, the model parachute hung up on the load measuring rod (see figure 11) upon re-inflation and suffered minor damage near the apex. During subsequent tests the angle of attack was held to a value that avoided model parachute collapse. It was easy to determine when the model parachute was about to collapse by observing it through the wind tunnel windows.

OBSERVATIONS

The following observations were made during test operations:

1) The drag and static stability test fixtures performed well as designed, yielding good data with acceptably low levels of scatter.

2) Model parachute vibrations, and the dynamic loads they imposed on the wind tunnel balances, placed limits on the conditions (i.e., dynamic pressure and Mach number) at which tests could be safely conducted. In general, model parachute vibrations increased with decreasing density and increasing Mach number for a given dynamic pressure. The wake of the model backshell seemed to have a significant effect on these vibrations; tests conducted without the backshell exhibited lower levels of vibration.

3) Model parachute wear was worst at the attachment to the swivel. A smooth interface between the suspension lines and the swivel was critical. The model parachutes used during the present investigation could be refurbished by replacing the suspension lines. This was found to be useful since the canopies lasted longer than the suspension lines.

4) At higher Mach numbers some model parachutes had a tendency to rotate. This tendency did not seem to be inherent to a particular model parachute (which might have indicated that the model parachute had a built-in asymmetry) since lowering the Mach number while maintaining the same dynamic pressure stopped the rotation.

5) A low-friction swivel was found to be important in avoiding suspension line twisting once a model parachute started rotating. To prevent rotation during static stability testing a thin Kevlar™ line was loosely tied from the edge of the disk to the rear truss.

DATA ANALYSES

BLOCKAGE CORRECTIONS

Wind tunnel test section walls impose artificial constraints about the test model. Slotted test section walls reduce the constraint but some wall interference, which is a function of the model solid blockage and the test section openness ratio, typically remains. The few reports in the open literature dealing with wall interference for parachute tests typically consider only solid wall test sections. Analytical wall interference correction techniques have been developed which use measured model forces and static pressures on the test section walls. One such correction technique, described in reference 5, has been successfully applied to conventional aircraft models in a porous test section. The development of the technique does not prohibit its use for a high blockage model such as a parachute. The technique requires the longitudinal static pressure distribution on all four walls of a square test section. Examination of the pressure distributions on the east and west walls showed them to be nearly the same. Thus, the static pressure on the west wall was used for all four walls. A typical wall pressure distribution and the associated dynamic pressure blockage correction factor, k_q, for the MPF model parachute fabricated from F-111 fabric is presented in figure 13. The value of k_q at the upstream edge of the model parachute band was used to correct the dynamic pressure. Note that the parachute has an effect well upstream of the canopy, yielding values of k_q less than one for stations between 60 and 67 ft. Calibration runs with an empty tunnel (i.e., no parachute) yielded the expected result that $k_q = 1$ and provided a partial validation of the blockage correction methodology. The values of the blockage correction factor, k_q, applied to the dynamic pressure

varied from approximately 1.02 to 1.07. A similar correction factor for the Mach number was also calculated. The Mach number derived from the wind tunnel instrumentation was multiplied by this correction factor which varied from approximately 1.01 to 1.04. All values of the Mach number reported in this paper were corrected in this way.

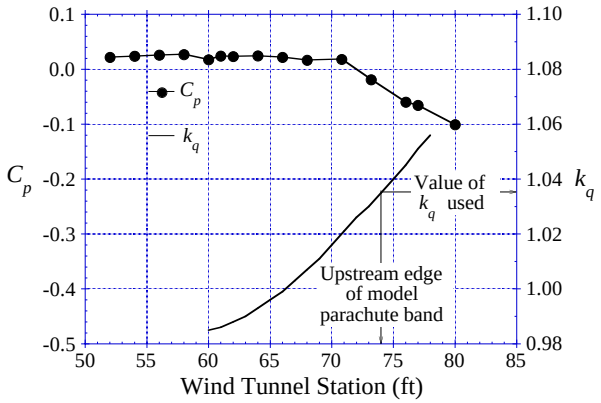

Figure 13 – Wall C_p and k_q vs wind tunnel station. MPF model parachute fabricated from F-111 fabric at M = 0.29 and q = 26 psf.

STRUT DRAG INTERFERENCE CORRECTIONS

The wake of the front strut upstream of the model parachute has the undesired effect of slightly reducing the measured magnitudes of the aerodynamic coefficients. To correct for this effect all measured forces and moments were multiplied by the factor $k_{\alpha S}$:

$$k_{\alpha s} = 1.0 + k_\alpha k_s \tag{1}$$

where,

$$k_s = 0.858 \frac{(C_D A)_{\text{strut}}}{S_P} \tag{2}$$

The quantity $(C_D A)_{\text{strut}}$ was an estimate of the strut drag area directly upstream of the projected model parachute diameter at an angle of attack of zero, and S_P was the projected model parachute area. The coefficient 0.858 was determined from experimental data obtained by varying the projected drag area of objects upstream of the model parachute at the front strut location. For the model parachutes tested in the present investigation k_S had values between 0.026 and 0.029. The parameter k_α accounted for the variation in front strut blockage as a function of angle of attack. During drag testing it was assumed that the model parachute was always directly downstream from the front strut, and for these tests k_α was set to a value of one. During static stability testing k_α was set to a value between zero and one (inclusive) depending on how much of the front strut was directly upstream of the model parachute.

DRAG DATA ANALYSES

The drag coefficient was calculated from the equation:

$$C_D = \frac{k_{\alpha S} D_{meas}}{k_q q_{meas} S_0} = \frac{D}{q S_0} \tag{3}$$

where D_{meas} is the drag measured by the wind tunnel balance and q_{meas} is the dynamic pressure calculated from the wind tunnel instrumentation. Note that D_{meas} is multiplied by the factor $k_{\alpha S}$ to account for the effects of strut drag interference, and q_{meas} is multiplied by the factor k_q to correct for blockage effects. The measured value of S_0 for each model parachute was used in the drag data analyses.

STATIC STABILITY DATA ANALYSES

From the two wind tunnel balances used during static stability testing, the forces and moments shown in figure 14 were measured. By summing both tangential force components, T_{front} and T_{rear}, the total measured tangential force component was determined and the tangential force coefficient, C_T, calculated from:

$$C_T = \frac{k_{\alpha S}\left(T_{front} + T_{rear}\right)}{k_q q_{meas} S_0} = \frac{T}{q S_0} \tag{4}$$

If the fitting at the apex of the model parachute had been frictionless (see figure 11), then T_{rear} would have been zero. In practice, T_{rear} accounted for a few percent of the total tangential force. Summing both normal force components, N_{front} and N_{rear}, the total measured normal force was determined and the normal force coefficient calculated from:

$$C_N = \frac{k_{\alpha S}\left(N_{front} + N_{rear}\right)}{k_q q_{meas} S_0} = \frac{N}{q S_0} \tag{5}$$

From N_{rear}, and the moment being measured by the rear wind tunnel balance about its moment center, M_{rear}, the location of the model parachute apex in front of the aft wind tunnel balance moment center, L_{rear}, could be calculated: $L_{rear} = M_{rear} / N_{rear}$. With this knowledge the location of N_{rear} in relationship to N_{front} could be determined given that the overall dimensions of the test

fixture were known. From statics the location of the center of pressure, X_{cp}, could then be determined, and the pitching moment about the suspension lines confluence point calculated:

$$C_m = -\frac{k_{\alpha S}\left(N_{front} + N_{rear}\right)X_{cp}}{k_q q_{meas} S_0 D_0} = \frac{m}{qS_0 D_0} \tag{6}$$

Note that C_N, C_m, X_{cp}, and D_0 are related by:

$$\frac{X_{cp}}{D_0} = -\frac{C_m}{C_N} \tag{7}$$

The measured values of D_0 and S_0 for each model parachute were used in the calculations for the static stability coefficients. Since L_{rear} and the test fixture dimensions were known, an accurate value of the model parachute length from the suspension lines confluence point to its apex, L, was calculated without resorting to photographic or video analyses. Figure 15 shows the sign convention and definition used for C_T, C_N, C_m, angle of attack (α), X_{cp}, and L.

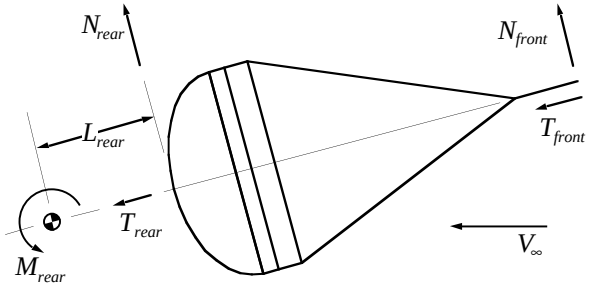

Figure 14 – Forces and moments measured during static stability testing.

The C_T, C_N, and C_m data presented in the results section was interpolated by splines which smoothed the experimental data (i.e., the spline did not have to pass through every point). Test data were usually collected for both positive and negative angles of attack. All data was "mirrored" about $\alpha = 0$ before fitting to the spline. This imposed a symmetry constraint on the C_T spline and anti-symmetry constraints on the C_N and C_m splines. From the splined data X_{cp} was calculated anew using equation 7.

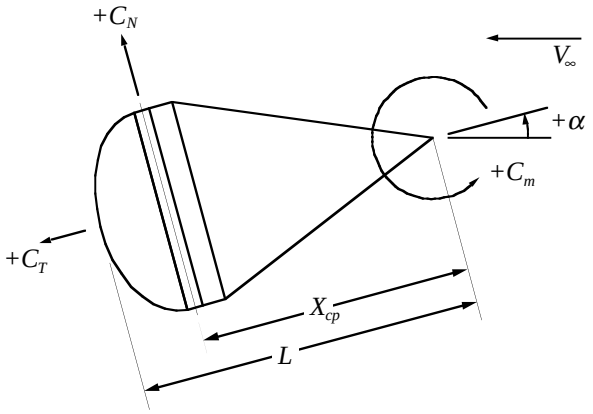

Figure 15 – Definition and sign convention for C_T, C_N, C_m, α, X_{cp}, and L.

GEOMETRIC AND TOTAL POROSITY CALCULATIONS

The geometric porosity, λ_g, was determined from the equation:

$$\lambda_g = \frac{A_V + A_G}{S_0} \tag{8}$$

where A_V and A_G are the areas of the vent and the gap, respectively. For the model parachutes the vent was partially blocked by test fixtures requirements, and the vent area was calculated from:

$$A_V = \pi\left(\frac{D_V}{2}\right)^2 - A_{block} \tag{9}$$

where A_{block} was the vent blockage induced by the test fixture requirements (i.e., 1.23 in^2). In the model parachutes D_V was adjusted to maintain geometric similarity in A_V with the corresponding full-scale MER parachutes. The gap area was calculated from:

$$A_G = \pi H_G \frac{\left(D_D + D_B\right)}{2} \tag{10}$$

Total porosity was determined from:

$$\lambda_t = \lambda_g + c_e\left(1 - \lambda_g\right) \tag{11}$$

where c_e was the effective porosity of the fabric. The effective porosity was estimated based on unpublished data provided by Pioneer Aerospace and a variation of the approach proposed by Lingard and Underwood[6] (the equivalent of equation 11 in reference 6 does not include $1 - \lambda_g$ in the second term). At a given operating condition a fictitious velocity, V_{fict}, was calculated from:

$$V_{fict} = \sqrt{\frac{2qC_D S_0}{\rho S_P}} \tag{12}$$

Where S_P is the parachute projected area. A Reynolds number per unit length, Re^*, was determined from this fictitious velocity:

$$Re^* = \frac{\rho V_{fict}}{\mu} \tag{13}$$

The effective porosity was then calculated from:

$$c_e = -\frac{k_2}{2k_1 Re^*} + \sqrt{\frac{k_2^2}{4k_1^2 Re^{*2}} + \frac{1}{2k_1}} \tag{14}$$

Where k_1 and k_2 were constants determined from a best fit of the available data. The original data used in estimating k_1 and k_2 was with a polyester fabric with a standard permeability of 148 CFM/ft^2. Values c_e for fabrics other than this one were estimated by calculating c_e for this polyester fabric, and then scaling c_e with respect to the ratio of standard permeabilities. Because there was some uncertainty in the permeability data used in determining k_1 and k_2, and the validity of scaling c_e with respect to standard permeability was not verified, there were concerns regarding the absolute accuracy of c_e as calculated by the process described above. However, this approach was considered to be adequate for the purpose of interpolating the wind tunnel test data to Mars flight conditions.

UNCERTAINTY ESTIMATES

Both the precision (i.e., random) and bias (i.e., systematic) uncertainties for all coefficients were calculated. Precision uncertainties were determined by considering the variation in results between runs conducted on different days with the same model parachute at the same operating conditions, and with different model parachutes of the same type at the same operating conditions. Bias uncertainties were calculated by applying the techniques of reference 7, using estimated values of the bias uncertainties for the various measurements (e.g., dynamic pressure, forces, etc.). Conservative values for all uncertainties were used. The lack of sufficient data, however, limited the accuracy of the stated uncertainties and they must be considered to be estimates. All uncertainties reported in this paper were estimated to the 99.7 percent confidence level of the mean (i.e., two-sided 3-sigma level for a normal distribution) and were assumed to follow a normal distribution.

INTERPOLATION OF RESULTS FOR MARS FLIGHT

Total porosity was calculated for the model parachutes fabricated from MIL-C-7020 Type III and F-111 fabric at the various test conditions, and for the full-scale MER parachute at Mars flight conditions. In all cases the total porosity for Mars flight conditions was found to be within the bounds established by the model parachute test results. Fabric permeability, and thus total porosity were found to be a key parameter affecting the model parachute aerodynamic coefficients. Thus, calculations for Mars flight conditions were performed by linearly interpolating the appropriate wind tunnel test results using total porosity as the interpolating variable.

RESULTS

MARS FLIGHT CONDITIONS AND TOTAL POROSITY

The Mars flight conditions of interest to the present investigation are shown in table 2. Note that the Martian atmosphere is composed mainly of CO_2. The corresponding total porosities for the full-scale MER parachutes at these conditions are given in table 3. For the total porosity calculations the full-scale MER parachutes were assumed to have a D_0 of 49.5 ft and a composite (i.e., combined disk and band) standard fabric permeability of 108 CFM/ft^2. These values of the total porosities were used to interpolate the drag and static stability coefficients at the corresponding Mars flight conditions.

Table 2 – Mars flight conditions.

	Terminal Descent	Heatshield Release
M	0.287	0.459
q (psf)	0.754	1.18
ρ (slugs/ft^3)	2.71 x 10^{-5}	1.81 x 10^{-5}
μ (slug/ft-s)	2.43 x 10^{-7}	2.64 x 10^{-7}

Table 3 – S_P/S_0, λ_g, and λ_t at Mars flight conditions for the full-scale MER parachutes.

	1.6 Viking	MPF
S_P/S_0	0.394	0.308
λ_g	0.111	0.093
λ_t at Terminal Descent	0.141	0.125
λ_t at Heatshield Release	0.144	0.127

GEOMETRIC RESULTS

From video camera data and other measurements, the geometric parameters shown in table 4 were determined.

Table 4 – Geometric parameters of the model parachutes.

Model Parachute	D_P/D_0	S_P/S_0	L/D_0
1.6 Viking MIL-C-7020 Type III	0.628	0.394	2.01
1.6 Viking F-111	0.612	0.375	2.00
MPF MIL-C-7020 Type III	0.555	0.308	2.06
MPF F-111	0.568	0.323	2.06

DRAG RESULTS

The test drag results for the 1.6 Viking and MPF model parachutes are shown in table 5 and figure 16. As can be seen from this table and figure, the 1.6 Viking design has a higher drag coefficient than the MPF design. This was expected since S_P/S_0 is larger for the 1.6 Viking model parachute. Previous drop tests[8] with full-scale parachutes also exhibited this relationship between percentage of projected area and drag coefficient. The model parachutes manufactured from F-111 fabric have lower total porosity and a higher drag coefficient (by 11 to 15 percent). This observation underscores the relationship between fabric permeability and drag coefficient. Figure 16 shows a 7 to 9 percent increase in the drag coefficient over the range of Mach numbers considered ($0.134 \le M \le 0.469$) although care should be exercised in the interpretation of this trend since there is also a slight variation in total porosity.

Interpolating these drag data to Mars flight conditions using total porosity as the interpolating parameter yields the results shown in table 6. Trends in the drag coefficient data similar to those already mentioned can also be seen in these results. Reconstructions of the drag coefficient based on the Mars Pathfinder flight data were performed by Witkowski[9] and Desai et al.[10] Their reconstructions yielded drag coefficients of 0.43 and 0.41, respectively, at a Mach number of approximately 0.3. These values are close to the drag coefficient value for the MPF parachute at Mars flight terminal descent condition obtained in the present investigation (i.e., $C_D = 0.405$ at $M = 0.29$). This comparison adds confidence to the validity of all estimates.

Table 5 – Summary of drag coefficient results.

Model Parachute	M	q (psf)	λ_g & λ_t	C_D
1.6 Viking MIL	0.134	26.67	0.115 0.178	0.440±0.026 (±5.9%)
1.6 Viking F-111	0.135	27.07	0.115 0.118	0.504±0.030 (±6.0%)
1.6 Viking MIL	0.291	26.25	0.115 0.177	0.457±0.027 (±5.9%)
1.6 Viking F-111	0.293	25.15	0.115 0.118	0.506±0.030 (±5.9%)
1.6 Viking MIL	0.465	25.22	0.115 0.175	0.477±0.028 (±5.9%)
1.6 Viking F-111	0.469	27.02	0.115 0.118	0.539±0.031 (±5.8%)
MPF MIL	0.135	26.70	0.094 0.160	0.363±0.022 (±6.1%)
MPF F-111	0.137	27.31	0.095 0.098	0.419±0.025 (±6.0%)
MPF MIL	0.292	26.37	0.094 0.158	0.376±0.022 (±5.9%)
MPF F-111	0.292	24.68	0.095 0.098	0.428±0.026 (±6.1%)
MPF MIL	0.462	34.54	0.094 0.158	0.396±0.021 (±5.3%)

Notes:
1) Model parachutes denoted MIL were fabricated using MIL-C-7020 Type III fabric. Model parachutes denoted F-111 were fabricated using F-111 fabric.
2) Uncertainty in C_D is estimated total (precision and bias) for the mean value at the 99.7 percent confidence level.

Table 6 – Interpolated drag coefficients for Mars flight conditions.

Condition	1.6 Viking C_D	MPF C_D
Terminal Descent M ≈ 0.29	0.486±0.027 (±5.6%)	0.405±0.023 (±5.7%)
Heatshield Release M ≈ 0.46	0.511±0.028 (±5.5%)	See note below

Notes:
1) Uncertainty in C_D is estimated total (precision and bias) for the mean value at the 99.7 percent confidence level.
2) There was insufficient data to interpolate for the MPF C_D at Heatshield Release.

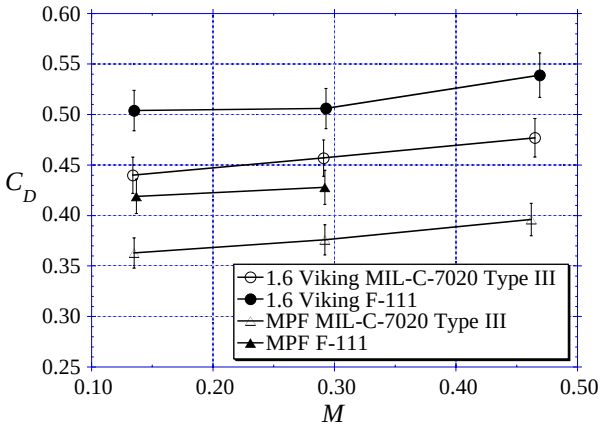

Figure 16 – Summary of drag coefficient results. Uncertainty bars are total for the mean at the 99.7 percent confidence level.

STATIC STABILITY RESULTS

A summary of the static stability test conditions and results is shown in table 7. Of particular interest in evaluating static stability was the statically stable trim angle of attack, α_{trim}. This was the angle of attack for which $C_m = 0$, and $dC_m/d\alpha < 0$. Two observations could be made from the values of $|\alpha_{trim}|$ listed in table 7. First, for both the 1.6 Viking and MPF model parachutes, those manufactured from F-111 fabric exhibited significantly larger values of $|\alpha_{trim}|$. This behavior was attributed to the lower permeability of F-111 fabric as compared to the MIL-C-7020 Type III fabric. Second, the MPF model parachutes had lower values of $|\alpha_{trim}|$ as compared to the 1.6 Viking model parachutes at equivalent test conditions. The source of this was the relative difference in band height between the MPF and 1.6 Viking model parachutes. These data verified qualitative observations made during earlier full-scale drop tests,[8] namely that DGB parachutes with larger values of H_B/D_0 have lower values of $|\alpha_{trim}|$. It was not possible to test the 1.6 Viking model parachute fabricated from F-111 fabric at $M = 0.29$ and $q \approx 25$ psf due to problems related to model parachute vibration. The highest Mach number achieved with this model parachute was 0.226 at a dynamic pressure of 15.50 as shown in table 7.

In figures 17 through 20 C_T, C_N, C_m, and X_{cp}/D_0 are plotted vs α for the MPF model parachute at $M = 0.29$, $q \approx 25.5$ psf and fabricated from either MIL-C-7020 Type III or F-111 fabric. These plots showed the general behavior for these quantities with respect to α, in addition to the trends with varying fabric permeability. The tangential force coefficient, C_T (shown in figure 17), exhibited the same trend noted earlier for C_D, namely that it was generally higher for model parachutes fabricated from F-111 fabric as compared to those fabricated from MIL-C-7020 Type III fabric at equivalent conditions. Figures 18 and 19 show clearly that the MPF model parachute fabricated from MIL-C-7020 Type III fabric was statically stable over the angle of attack range investigated, whereas those fabricated from F-111 fabric were statically unstable at $\alpha = 0$ and had a nonzero $|\alpha_{trim}|$. The calculated nondimensional center of pressure, X_{cp}/D_0, shown in figure 20 exhibited

Table 7 – Summary of static stability test conditions and $|\alpha_{trim}|$ results.

Model Parachute	M	q (psf)	λ_g & λ_t	$\lvert\alpha_{trim}\rvert$
1.6 Viking MIL	0.105	16.07	0.115 0.178	2.0°
1.6 Viking F-111	0.104	15.82	0.115 0.118	16.2°
1.6 Viking MIL	0.293	25.87	0.115 0.177	1.8°
1.6 Viking F-111	0.226	15.50	0.115 0.118	16.3°
MPF MIL	0.105	16.11	0.095 0.159	0.0°
MPF F-111	0.106	16.41	0.095 0.098	12.1°
MPF MIL	0.291	25.34	0.095 0.158	0.0°
MPF F-111	0.294	25.54	0.095 0.098	8.5°

Note: Model parachutes denoted MIL were fabricated using MIL-C-7020 Type III fabric. Model parachutes denoted F-111 were fabricated using F-111 fabric.

some unusual behavior which may not have been physically real. For the model parachute fabricated from F-111 fabric there was a singularity near $|\alpha_{trim}| = 8.5°$. Considering equation 7 it was clear that this occurred because $C_N = 0$ but $C_m \neq 0$ at the singularity angle of attack. Having this occur is physically possible. However it is just as likely that this occurred due to the way in which the data was splined, yielding slightly different values of the angle of attack for which C_N and C_m were zero. The X_{cp}/D_0 vs α curve for the model parachute fabricated from MIL-C-7020 Type III fabric exhibited similar behavior at $\alpha = 0$. Although the reason for this singularity was not particularly important, it did indicate that using C_N and C_m instead of C_N and X_{cp} in numerical simulations would avoid the problem of dealing with this

singularity. Figure 21 compares the C_m vs α curves for the MPF and 1.6 Viking model parachutes fabricated from MIL-7020-C Type III fabric at M = 0.29 and $q \approx 25.5$ psf. The MPF parachute exhibited greater static stability over the range of angles of attack investigated. It is interesting to note that qualitative observations of the model parachutes motion during drag testing (where the model parachute apex was not constrained) agreed with the observations made here based on the static stability data.

The static stability data was interpolated (as described earlier) to predict the full-scale MER parachute behavior at the Mars flight terminal descent condition (M = 0.29) for both the 1.6 Viking and MPF parachutes. A summary of the trim angles of attack for these interpolations are given in table 8. The uncertainty boundaries 1 and 2 are total for the mean at the 99.7 percent confidence level. Because the interpolation depended on the calculation of the

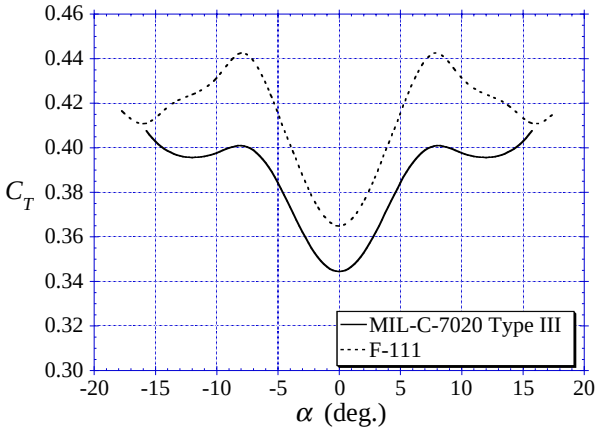

Figure 17 – C_T vs α for MPF model parachute at M = 0.29 and $q \approx 25.5$ psf.

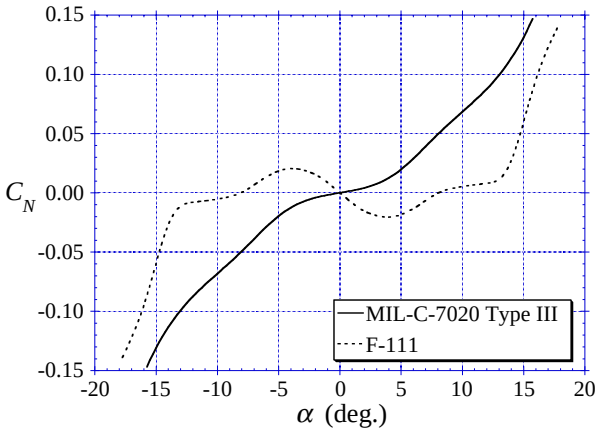

Figure 18 – C_N vs α for MPF model parachute at M = 0.29 and $q \approx 25.5$ psf.

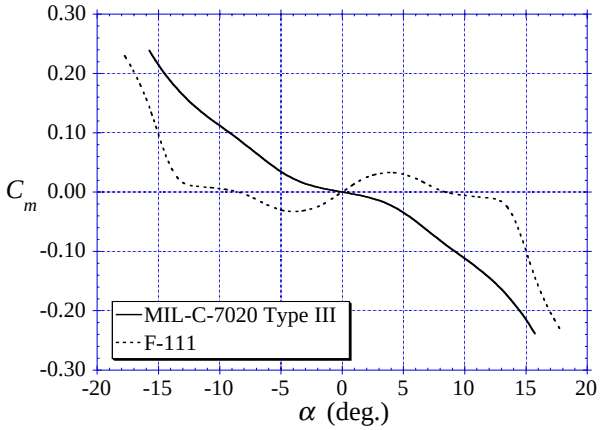

Figure 19 – C_m vs α for MPF model parachute at M = 0.29 and $q \approx 25.5$ psf.

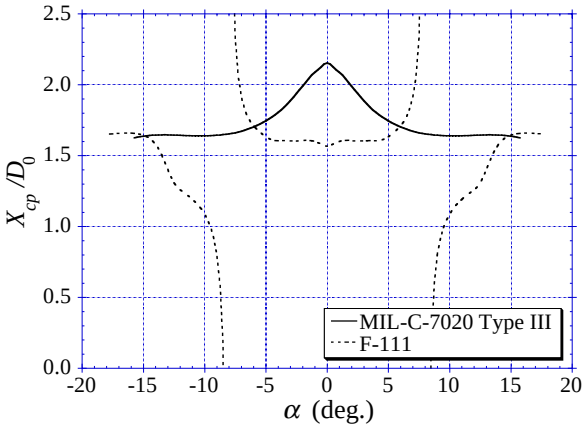

Figure 20 – X_{cp}/D_0 vs α for MPF model parachute at M = 0.29 and $q \approx 25.5$ psf.

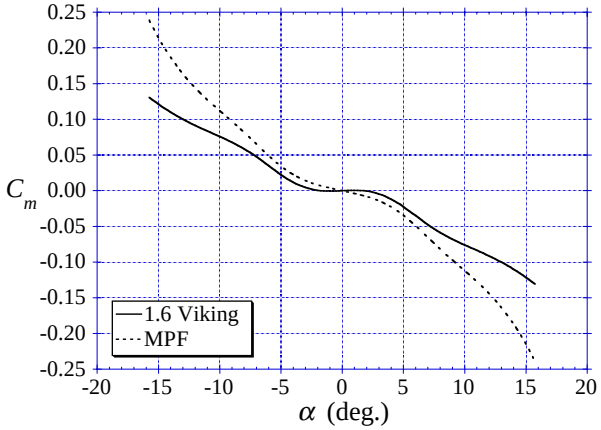

Figure 21 – C_m vs α for 1.6 Viking and MPF model parachutes at M = 0.29 and $q \approx 25.5$ psf. Both model parachutes manufactured from MIL-C-7020 Type III fabric.

effective fabric porosity for both the model and full-scale MER parachutes, an extra allowance was made in the estimation of the effective fabric porosity uncertainty in the calculation of the uncertainty boundaries. The C_T, C_N, and C_m vs α interpolations for the full-scale MER MPF parachute are shown in figures 22 through 24. Because most of the uncertainties in these parameters had common sources, it is likely that the uncertainties were highly correlated. Thus, if the "Uncertainty Boundary 1" curve for C_T was selected for an analysis, then the "Uncertainty Boundary 1" curves should also be used for C_N and C_m.

CONCLUDING REMARKS

The results presented here confirmed and quantified the observations made during the earlier drop test program[8] that increasing the relative height of the band in a DGB parachute decreased the drag and improved the static stability as defined by $|\alpha_{trim}|$. Although it was expected that the drag and static stability coefficients would be affected by fabric permeability, the magnitude of its effect was surprisingly large. This points out the importance of obtaining accurate data on the fabric porosity at the appropriate conditions and for the relevant gases when predicting the behavior of parachutes for operations in low-density planetary atmospheres.

Table 8 – Interpolated $|\alpha_{trim}|$ at Mars flight terminal descent condition (M = 0.29).

	1.6 Viking	MPF
Uncertainty Boundary 1	10.2°	6.4°
Interpolated Best Estimate	7.5°	5.2°
Uncertainty Boundary 2	6.0°	3.8°

Note: In the interpolation for the 1.6 Viking parachute, the data for the F-111 model parachute at M = 0.226 and q = 15.50 psf was used. See text and table 7.

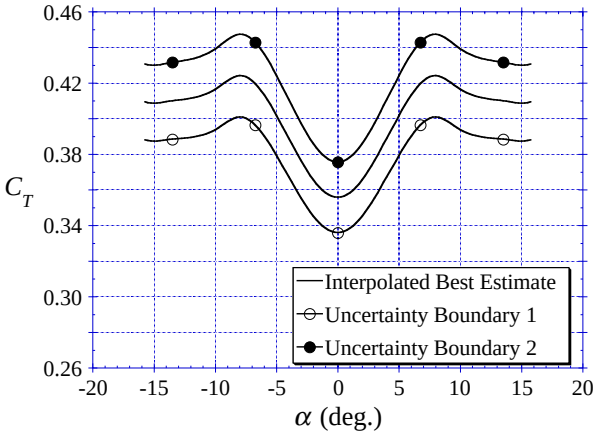

Figure 22 – Interpolated C_T vs α for the full-scale MER MPF parachute at terminal descent Mars flight condition (M = 0.29).

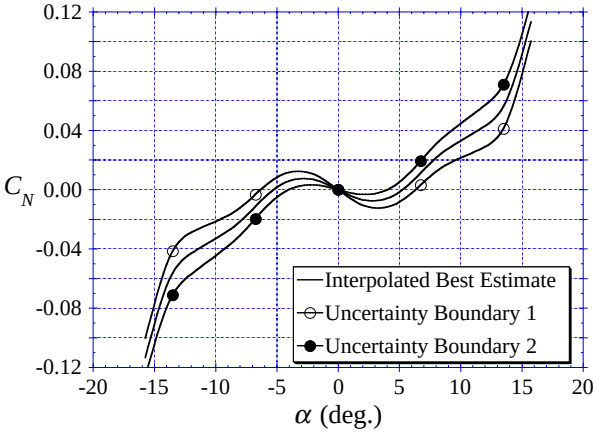

Figure 23 – Interpolated C_N vs α for the full-scale MER MPF parachute at terminal descent Mars flight condition (M = 0.29).

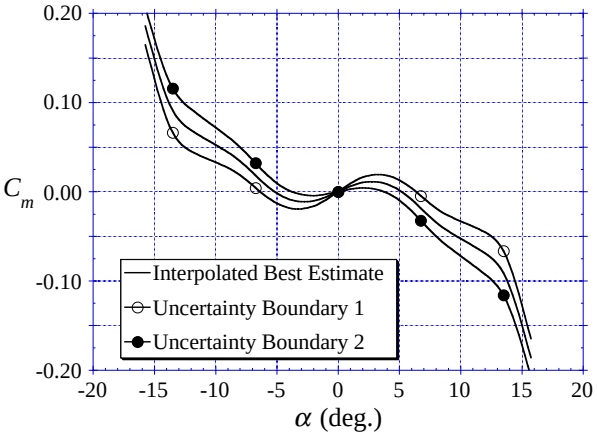

Figure 24 – Interpolated C_m vs α for the full-scale MER MPF parachute at terminal descent Mars flight condition (M = 0.29).

ACKNOWLEDGEMENTS

The authors would like to acknowledge the contributions of the following individuals. Robin Bruno, Adam Steltzner, and Wayne Lee of the Jet Propulsion Laboratory for their support of the research reported here. Al Witkowski, Jim Reuter, Yaro Taeger, and Ray Vasas of Pioneer Aerospace for the model parachutes and their technical support during testing. Carl Peterson of Sandia National Laboratories for his

support during test planning and execution. The NASA LaRC Aeroelasticity Branch staff, and the engineering and technical staff of the TDT for their support during test planning and execution.

REFERENCES

1) Gillis, C. L., "The Viking Decelerator System – An Overview," AIAA Paper 73-442, 1973.

2) Fallon II, E. J., "System Design Overview of the Mars Pathfinder Parachute Decelerator Subsystem," AIAA Paper 97-1511, 1997.

3) Steltzner, A., Lee, W., Bruno, R., and Desai, P., "The Mars Exploration Rovers Entry Descent and Landing Phase and the Use of Aerodynamic Decelerators," AIAA Paper 2003-2125, 2003.

4) Jaremenko, I., Steinberg, S., and Faye-Petersen, R., "Scale Model Test Results of the Viking Parachute System at Mach Numbers from 0.1 Through 2.6," NASA CR 149377, 1971.

5) Mokry, M., "Evaluation of Three-Dimensional Wall Interference Corrections from Boundary Pressure Measurements," National Research Council of Canada, Technical Report LTR-HA-51, November, 1980.

6) Lingard, J. and Underwood, J., "The Effect of Low Density Atmospheres on the Aerodynamic Coefficients of Parachutes," AIAA Paper 95-1556, 1995.

7) Coleman, H. W. and Steele, W. G., *Experimentation and Uncertainty Analysis for Engineers*, John Wiley & Sons, 1989.

8) Taeger, Y. and Witkowski, A., "A Summary of Dynamic Testing of the Mars Exploration Rover Parachute Decelerator System," AIAA Paper 2003-2127, 2003.

9) Witkowski, A., "Mars Pathfinder Parachute System Performance," AIAA Paper 99-1701, 1999.

10) Desai, P., Schofield, J., and Lisano, M., "Flight Reconstruction of the Mars Pathfinder Disk-Gap-Band Parachute Drag Coefficient," AIAA Paper 2003-2126, 2003.